# Thermal Fluctuations in the Structure of Naturally Chiral Pt Surfaces

Aravind Asthagiri[1], Peter J. Feibelman[2], and David S. Sholl[1,*]
[1] Department of Chemical Engineering, Carnegie Mellon University
Pittsburgh, PA 15213, USA
[2] Sandia National Laboratories, Albuquerque, NM 87185-1413, USA



In preparation for *Topics in Catalysis*

* Corresponding author: Fax: 412-268-7139. Email: sholl@andrew.cmu.edu

## ABSTRACT

The intrinsic chirality of metal surfaces with kinked steps (e.g. Pt(643)) endows them with enantiospecific adsorption properties (D. S. Sholl, *Langmuir*, 14, **1998**, 862). To understand these properties quantitatively the impact of thermally-driven step wandering must be assessed. We derive a lattice-gas model of step motion on Pt(111) surfaces using diffusion barriers from Density Functional Theory. This model is used to examine thermal fluctuations of straight and kinked steps.

**Keywords:** chiral, stepped surfaces, step fluctuations, Density Functional Theory

**Short Title:** Fluctuations in Pt Step Edges

## DISCLAIMER

## Section 1: Introduction

Stepped surfaces are of chemical interest because their exposed low-coordination sites may have an important effect on catalytic activity and selectivity. Surfaces cut to expose an array of kinked steps are a particularly exciting example, because kinks are intrinsically chiral [1-7], and thus provide an environment where the different enantiomers of chiral molecules can be expected to have different adsorption geometries, energies and reactivities [1,3-7]. For example, the electro-oxidation of *D*-glucose over a Pt(643) electrode differs from that of *L*-glucose over the same electrode because of the intrinsic chirality of the Pt(643) surface [3,4]. It is not hard to imagine many interesting processing applications, such as enantioselective catalysis and enantioselective crystallization, based on these naturally chiral surfaces.

Because their enantiospecific properties depend on ordered local arrangements of surface atoms, it is important to develop an atomic-scale understanding of chiral surface structure under practical conditions. In previous theoretical studies, chiral surfaces have been modeled as perfectly ordered high Miller index planes [1,5-7], an assumption whose approximate validity is confirmed by low energy electron diffraction (LEED) [2-4,6]. Nonetheless, stepped surfaces must deviate from their ideal structure due to thermally induced step wandering. For a recent review of step fluctuations, see Ref. [8]. In order to understand how step wandering will affect the enantiospecific adsorption properties of naturally chiral metal surfaces, it is first necessary to predict the structures of chiral surfaces after step fluctuations have occurred. Although the qualitative theory of step fluctuations is very well developed [8], accurate prediction of step structures for metal surfaces with atomic resolution remains challenging.

The aim of this paper is to develop a model that faithfully represents atomic motion along step edges on Pt surfaces and serves as a tool for characterizing the effects of step wandering on naturally chiral Pt surfaces. The surface structures generated by this model can then be used to assess the effect of step fluctuations on the enantiospecific adsorption of chiral organic molecules on chiral Pt surfaces [9]. The paper is structured as follows. In section 2 we describe how we use energy barriers computed via density functional theory (DFT) to parameterize a lattice gas (LG) model of Pt step dynamics. The parameterization's simplicity allows us to simulate step edges comprised of thousands of atoms on experimentally relevant time scales. In section 3 we demonstrate the accuracy of our theoretical approach by comparing our DFT and LG results to previous experimental measurements of step roughening for straight steps on Pt surfaces. The results of applying our model to the kinked Pt steps that are characteristic of chiral Pt surfaces are described in section 4. We conclude with a discussion of our results and prospects for future work in section 5.

**Section 2: Lattice Gas Model of Pt Step Dynamics**

Quantitative modeling of surface step fluctuations is challenging because one must account for the thermally driven mass transport of thousands of surfaces atoms over long time scales. Much progress has been made in this area by using atomically-based lattice models and coarse-grained continuum models [8]. A limitation of existing models is that they are based on simplified representations of the bond strengths and energy barriers to atomic diffusion. To model specific materials, it is obviously of value to replace these simplified models with more detailed models when possible. The possibility of applying density functional theory (DFT) to periodic systems containing hundreds of atoms offers

an attractive tool for developing these refined models. In this section, we describe how we have used DFT to parameterize a lattice gas (LG) model for step dynamics on Pt surfaces.

We restrict our work to stepped surfaces vicinal to Pt(111) which are known not to reconstruct below 800K [3,4,10,11] and which when cut to expose kinked steps, are intrinsically chiral [1,3-5]. Straight steps on these surfaces have one of two orientations. Those that form a (100) microfacet are referred to as A steps while those forming (111) microfacets are B steps [10,12]. Surfaces with steps that alternate between A and B, such as the Pt(854) surface shown in Fig. 1, are chiral [1-4].

One of us recently performed an extensive *ab initio* study of Pt atom diffusion along the bottom of steps on these surfaces [12]. Confirming the importance of calculating diffusion energetics via DFT, the computed energy barriers for diffusion of a Pt atom along straight A or B steps are roughly three times larger than the diffusion barrier on a bare Pt(111) surface - quite different, for example, from what one would imagine in a bond-counting picture. In addition, the diffusion barriers along A and B steps differ, even though an atom adjacent to a step edge has the same number of nearest neighbors independent of the step's identity. The DFT results are in good agreement with experimental measurements of barriers for diffusion on Pt(111) and Pt(331) [12]. It is also noteworthy that these barriers are not correctly predicted by current semi-empirical potentials [12].

Despite the predictive power of DFT, it is not practical to compute energy barriers directly for all processes that can contribute to step roughening via thermal fluctuations. Thus, we derive a LG model for diffusion of Pt atoms along step edges that embodies all

of the energy barriers currently known from DFT calculations. Four assumptions make this approach feasible. First, we assume that all atomic motion along step edges takes place by single Pt atoms hopping between adjacent local energy minima on the surface. That is, we do not include any multi-atom diffusion pathways such as concerted substitution. DFT results indicate that while concerted substitution can occur along Pt step edges, the barriers to these events are significantly higher than for single atom hopping [12]. Second, we assume that Pt atoms cannot escape from a step edge onto an adjacent terrace. In the terminology of the step fluctuation literature, we allow only periphery diffusion. This assumption is based on the observation that the energy barriers for an atom moving from a step edge to a terrace are larger than those for motion along the step edge [13]. Third, the energy barriers for removing Pt atoms from seven- or eight-fold coordinated positions *in* the step edge are assumed to be large enough that these processes can be ignored. For the perfect Pt(854) structure shown in Fig. 1, for example, this assumption means that only the six-fold coordinated kink atoms are considered to be mobile. Finally, the rate of each process is assumed to have the form $k = \nu \exp(-E_b / k_B T)$, where the pre-exponential factor is fixed to be $\nu = 10^{13}\,\mathrm{s}^{-1}$ for all processes and $E_b$ is the process-dependent activation energy.

We noted above that simple bond counting schemes do not even qualitatively describe Pt self-diffusion on stepped surfaces. To extend the energy barriers computed with DFT to give a LG model that can accurately describe any diffusion event subject to the assumptions listed above, we have developed an extended bond counting method that characterizes the local environment of the moving atom. In this model, each diffusion activation energy has the form $E_b = E^{TS} - E^{S}$, where $E^{TS}$ and $E^{S}$ are the atom's energy

at the transition state and step edge local minima, respectively. To reflect the mobile atom's local geometry, nearest-neighbor Pt atoms in the step edge are identified as being either A, B, 120° corner, 240° corner, 300°A corner, and 300°B corner atoms, as indicated in Fig. 2. $E^S$ is then defined by

$$E^S = \sum_{i=1}^{6} N_i E_i^S, \qquad (1)$$

where the index $i$ runs over the 6 types of neighbors, $N_i$ is the number of nearest neighbors of type $i$ and $E_i^S$ indicates the interaction energy of the mobile atom with a neighbor of type $i$. Transition state energies are defined using a variation on Eq. (1). We define any nearest neighbor atom that is present in both the initial and final minimum energy states as a full bond and any nearest neighbor present in only one of the minima as a partial bond. The transition state energy is then defined as

$$E^{TS} = \sum_{i=1}^{6} (N_i + \gamma M_i) E_i^{TS}. \quad (2)$$

Here, $N_i$ and $M_i$ are the number of full and partial bonds for the process, respectively, and $E_i^{TS}$ is the interaction energy with a neighbor of type $i$. Equations (1) and (2) define a system involving 13 parameters that must be fit to DFT data. The DFT data comprise 18 transitions involving 4 of the 6 neighbor types (A, B, 120° corner, and 240° corner) we have identified. The 300°A and 300°B corner type atoms occur at the intersection of A-A steps and B-B steps respectively. These structures do not appear on any Miller index surface of Pt. In principle, these two structures may occur if the thermal roughening is severe, but in the simulations discussed in section 4 we have not seen this development. Nevertheless, to complete the picture of diffusion along steps we include the atom types associated with these corners in Eqs. (1) and (2). The energy barriers for diffusion

around 300°A and 300°B corners have not been computed using DFT, so we estimate these barriers based on similar transitions found at the A-B step intersections.

Inserting the DFT barriers into Eqs. (1) and (2) yields a system with 22 equations and 13 unknowns. Once $\gamma$ is fixed, the resulting system can be solved using linear least squares. One useful fact is that the estimated barriers for 300°A and 300°B corners only influence the 4 unknowns involving the same corners, so these estimated barriers do not affect the parameters associated with other atom types. Table 1 shows a comparison of the predicted energy barriers to both the LDA and GGA DFT data for an optimal parameter set. Table 2 shows the values of the parameters used to determine the energy barriers from the correlation function. In Table 1, different types of energy barriers are distinguished by denoting energy minima on A steps, B steps, corners, and kinks of steps from Miller index surfaces by A, B, C, and K, respectively. In some cases, the energy barrier depends not only on the initial and final state but also on a third state accessible from either the initial or final states. These cases are shown in Table 1 by placing this third state in parentheses.

Many features of Pt diffusion along step edges are accurately represented by our model. For example, the model captures the DFT prediction that the barrier to diffusion along an A step is approximately 0.05 eV lower than for diffusion along a B step. Not all barriers are represented so accurately. LDA predicts that the energy barrier to move from a kink site to an A step (1.27 eV) is 0.14 eV lower than to move from a kink site to a B step (1.41 eV). In our model, these two barriers are 1.32 and 1.34 eV respectively, *i.e.* the difference between them is greatly reduced. The root mean square (RMS) deviation between the LDA results and the results of our model in Table 1 is 0.032 eV, compared

ref. #12

to an estimated uncertainty of ±0.02 eV in the DFT results [Feibelman99]. Parameterizing our model using GGA barriers yields a RMS deviation of 0.029 eV. The final parameters used in Eqs. (1) and (2) are listed in Table 2. This model gives a LG model for self-diffusion along Pt step edges that is directly based on energy barriers computed using DFT and, as we will show in section 4, can be used to perform practical simulations of Pt step roughening.

**Section 3: Thermal Fluctuations in Straight Step Edges**

Although we are ultimately interested in modeling fluctuations in kinked steps on naturally chiral Pt surfaces, we begin by applying our model to straight step edges. This allows us to introduce some necessary terminology and, more importantly, compare our results to existing experimental data.

To describe fluctuations of surface steps succinctly, it is convenient to define $x$ and $y$ axes in the surface plane such that $y$ measures distance along a step edge (in lattice units) and $x$ measures displacement of the step from its initial position. This coordinate system is illustrated for a kinked step in Fig. 3. The time dependent position of a step is written in these coordinates as $x(y,t)$. The main measure of step fluctuations we will consider here is the temporal correlation function,

$$G(t) = \left\langle [x(y,t) - x(y,0)]^2 \right\rangle. \quad (3)$$

Theoretical and experimental studies of step fluctuations have established that $G(t) \propto t^{\alpha}$, with the scaling exponent $\alpha$ depending on the physical mechanism of mass transport [8,10]. Langevin analysis of models of step fluctuations via periphery diffusion, evaporation-condensation, and step-step diffusion predict that $\alpha$ =1/4, 1/3, and 1/2, respectively [8,14]. Experimental observations of thermal fluctuations of straight A and B

steps on Pt surfaces have revealed that $\alpha \approx 1/4$ for temperatures up to 800 K, suggesting that step fluctuations at these temperatures are dominated by periphery diffusion [10].

Fluctuations of straight steps due to periphery diffusion can be quantitatively analyzed in terms of the energy barriers for atomic motions along the step edge. In this section, we perform this analysis using the DFT barriers described in section 2 and compare our results to the experimental data of Giesen *et al.* [10]. We concentrate on the temperature dependence of *G(t)* by writing

$$G(t) = \nu \exp\left(-\frac{E_{eff}}{k_b T}\right) t^{1/4}. \quad (4)$$

Using experimental data taken between 540 and 800 K, Giesen *et al.* measured the effective energy barrier in this expression to be 0.50 ± 0.04 eV for both A and B steps [10]. The observation that both steps give the same barrier (within the experimental uncertainty) is inconsistent with experimental data on equilibrium island shapes on Pt(111) [15] and with recent DFT calculations of kink- and step-formation energies [16]. This inconsistency has led to the suggestion that Giesen *et al.* may not have been able to distinguish between A and B step orientations in the experiments [16]. In this case, the experimental results would be an average of the separate results for A and B steps. We return to this point below.

To compare $E_{eff}$ to the DFT barriers discussed in section 2, we note that scaling theories predict [10,17,18]

$$G(t) \propto (b^2)^{3/4} (D_s)^{1/4} t^{1/4}, \quad (5)$$

where $D_s$ is the diffusion coefficient for mass transport along the step and $b^2$ is the so-called step-diffusivity. If we denote the difference in energy between an atom located at a

kink site on the step edge and an isolated adatom on the step edge by 2ε, the step diffusivity obeys $b^2 \propto \exp(-\varepsilon / k_B T)$ [10]. When the concentration of isolated adatoms on the step edge is low, as it is for straight Pt steps below 800 K, $D_s = D_{tr} \exp(-2\varepsilon / k_B T)$, where $D_{tr}$ is the tracer diffusion coefficient of a single atom hopping along the step edge [10,19]. Natori and Godby showed that this tracer diffusion coefficient can be calculated analytically when the potential energy surface traversed by an atom while diffusing past a kink has the form shown in Fig. 4 if the kinks are equally spaced [20]. Taking this kink spacing on a real surface to be the average kink spacing gives

$$D_{tr} = \frac{n^2 \Gamma_d}{(n-1+1/S)(n-1+\Gamma_d/\Gamma_a)}, \quad (6)$$

where $n = (1/2)\exp(+\varepsilon / k_B T)$ is the average spacing in lattice units between step kinks [10], and $\Gamma_d = \Gamma_0 \exp(-E_d / k_B T)$, $\Gamma_a = \Gamma_d \exp(-2\varepsilon / k_B T)$, and $S = \exp(-\Delta / k_B T)$ are defined using the energy barriers labeled in Fig. 4 [10,20]. $\Gamma_0$ is a pre-exponential factor assumed to be constant for all hopping processes included in the Godby model. Noting that $n >> 1$ for the systems of interest, Eq. (6) simplifies to [10]

$$D_{tr} = \frac{\Gamma_o \exp(-E_d / k_B T)}{(2\exp(\varepsilon / k_B T) + 4\exp(\Delta / k_B T))}. \quad (7)$$

Combining Eqs. (5)-(7), we find that

$$G(t) \propto \left\{1 + 2\exp([\Delta - \varepsilon]/k_B T)\right\}^{1/4} \exp\left(-\left(\frac{3}{2}\varepsilon + \frac{1}{4}E_d\right)/k_B T\right) t^{1/4}. \quad (8)$$

Comparing this expression to Eq. (4), we see that the effective energy barrier measured by Giesen *et al.* is a nontrivial combination of a variety of microscopic energy barriers.

To apply the microscopic DFT barriers for diffusion at Pt step edges to Eq. (8), we first note that the potential energy surface shown in Fig. 4 is a simplification of the true situation, which is illustrated in Fig. 5 for an A step (the B step, not shown, is similar). The main difference between the Godby model and the actual potential energy surface is that the Godby model only identifies two energetically distinct minima while three distinct sites have been identified using DFT. The third site is a locally stable minimum that occurs as an atom diffuses around a corner (C) site (see Fig. 5). To reconcile the differences between Figs. 4 and 5, we analytically solve the population master equations [21] for a diffusing atom initially located at site K. For the situation shown in Fig. 5, absorbing boundary conditions are applied in the S sites available from sites C and K. The same boundary conditions are applied in the two S sites available from site K in Fig. 4. It is an excellent approximation to represent the decay of the population in site K of Fig. 5 by $\exp(-k_{tot}t)$, where $k_{tot}$ is the sum of the hopping rates from site K to the two relevant S sites. This is precisely the functional form of the analytic solution for Fig. 4, so the calculated $k_{tot}$ is used to define $\Delta$ and $E_a$ in Fig. 4. Performing this calculation at a range of temperatures shows that $\Delta$ and $E_a$ are very slightly temperature dependent. It is useful to note that the numerical results quoted below do not change appreciably if $E_a$ is simply fixed to be the highest energy barrier along the path K → C → S in Fig. 5.

Once the relevant microscopic energy barriers are specified, we determine $E_{eff}$ by plotting the right hand side of Eq. (8) over the temperature range of Giesen *et al.*'s experiments and fitting this result using Eq. (4). For B steps, this yields $E_{eff} = 0.61$ and 0.50 eV using barriers determined using LDA and GGA, respectively. For A steps, LDA

and GGA barriers lead to $E_{eff}$ = 0.52 and 0.39 eV, respectively. As noted above, the only available experimental measurement of $E_{eff}$ gave 0.50 +/- .04 eV for both A and B steps [10]. Noting that LDA and GGA barriers for Pt have previously been observed to over- and under-estimate experimentally observed results slightly [22,23], we see that DFT provides good predictions for the temperature dependence of straight step fluctuations on Pt surfaces. The only discrepancy between the theoretical and experimental results is that the latter predicts that the effective energy barrier for A and B steps is not the same. This observation is consistent with detailed DFT calculations of step- and kink-formation energies [16] and with the observed anisotropy of Pt island shapes on Pt(111) [15]. Our results lend weight to the possibility that the orientation of the steps in Giesen *et al.*'s experiments were not correctly identified, since the effective energy barrier observed in these experiments is completely consistent with an average of the theoretical values for the two types of steps. It would be interesting to reexamine this issue experimentally in a way that rules out any possible ambiguity in the step orientations.

Because our LG model predicts slightly different energy barriers than DFT, the values of $E_{eff}$ for our LG model deviate slightly from the DFT predictions above. Performing the same analysis as above using our LDA-based (GGA-based) LG model yields $E_{eff}$ =0.57 (0.44) eV for A steps and 0.56 (0.45) eV for B steps. These energy barriers are also consistent with the experimental results, but the difference between the A and B step results found using the DFT barriers directly is no longer present. This discrepancy occurs because our LG model does not accurately capture the difference between energy barriers from a kink site to the two types of step edges, $E_d$ in Eq. (8) (see section 2). Since these processes are rate limiting steps for diffusion along step edges,

they play an important role in the overall rates of thermal roughening. Despite these quantitative discrepancies, the overall agreement between the experimental data and our DFT-based LG model gives us confidence that we can use this model to assess fluctuations in more complex steps such as those treated in the following section.

**Section 4: Thermal Fluctuations in Kinked Step Edges**

We reiterate that the major thrust of our work is to develop accurate models of thermal step fluctuations on chiral Pt surfaces. To allow us to pursue a detailed examination of enantiospecific adsorption on thermally roughened chiral surfaces in the future, we need to generate roughened surfaces for which we know the location of each atom. For this reason, we have used Monte Carlo methods to simulate our LG model rather than extend the type of scaling analysis used above to kinked steps. In this section we describe our MC simulations and demonstrate some of the information that can be derived from them.

The LG model defined in section 2 reduces atomic motions to discrete hops between lattice sites with hopping rates determined by the local environment. The dynamics of models of this type can readily be realized using Kinetic Monte Carlo (KMC) simulations. We have simulated our model using the N-fold way [24], an efficient algorithm for simulating systems containing disparate hopping rates, as ours does. With this algorithm we can routinely simulate systems comprised of thousands of step edge atoms on experimentally relevant time scales. In all of the simulations discussed below, we consider a single isolated step on a Pt(111) surface that initially has a periodic array of kinks. We will denote initial steps that alternate between A steps $n$ atoms long and B steps $m$ atoms long as $(n,m)$ steps. For example, the step edges on the Pt(854) surface (see Fig. 1) are (3,1) steps.

The step temporal correlation function, *G(t)*, for (3,1) steps is shown for several temperatures in Fig. 6. Each data set in Fig. 6 was averaged over 3 independent trajectories for an initial step of length 2128 atoms and 532 initial kinks. Since thermal roughening is an activated process, the time scale for step wandering decreases rapidly as temperature is increased. As noted above, Langevin analysis of models of step fluctuations via periphery diffusion predicts that $G(t) \propto t^{1/4}$ [8,14]. Figure 6 shows that the results from our MC simulations are well described by the power law expression $G(t) \propto t^{\alpha}$, with $\alpha$ slightly less than 1/4. The scaling exponents obtained from applying our simulations to a range of steps are summarized in Table 3. In each case we found $\alpha$ by performing a least squares fit to data equally spaced in *ln(t)*. The uncertainty estimates in Table 3 are one standard deviation about the mean $\alpha$ determined from fitting 3-5 KMC trajectories independently. All the exponents in Table 3 are slightly less than 1/4 , indicating a systematic deviation between the models used for Langevin analysis of these systems and our more detailed model. Although this deviation is interesting from a theoretical point of view, it appears to be considerably too small to be resolved experimentally [10].

Power law growth of *G(t)* only occurs on sufficiently long time scales [8]. The time that must pass before beginning power law growth increases as temperature and is reduced as the distance between kinks along the step edge is increased. This can be seen by comparing *G(t)* for (3,1) steps (see Fig. 6) with similar data for (1,10) steps (see Fig. 7). In Fig. 6, power law growth is established very rapidly, even at $T = 450$ K. For (1,10) steps, there are considerable deviations from power law growth at early times for $T$ as high as 650 K (see Fig. 7). Only at $T = 700$ K does power law growth appear rapidly. If

each set of data in Fig. 7 is fitted to a single power law exponent, the exponents for $T <$ 700 K are considerably larger than 1/4 because of the accelerated growth in $G(t)$ at short times. We have performed simulations using steps that were allowed to evolve for long periods of time before fixing the initial configuration used to define $G(t)$ and observed similar results. This behavior has been seen previously in KMC simulations of step fluctuations based on simple bond-counting models [19]. It can also be seen in the experiments of Giesen *et al.* on straight steps on Pt(111) [10], where $\alpha$ decreased from .37 at 607 K to .24 at 800 K, with the lower temperature data showing the same type of curvature seen in Fig. 7.

The experimentally observable energy barrier $E_{eff}$ can be found by plotting $G$ at a fixed time at various temperatures [10]. The results of applying this procedure to (1,1), (2,1) and (3,1) steps are shown in Fig. 8. Each data point in Fig. 8 is the average of 3 KMC trajectories of steps with 532 initial kinks. The observed values of $E_{eff}$ for (1,1), (2,1) and (3,1) steps were 0.35, 0.33, and 0.29 eV, respectively. Very similar results were observed for (1,2) and (1,3) steps. Experimentally, Giesen *et al.* observed $E_{eff} = 0.50$ +/- .04 eV for straight steps [10] (see section 3). It is not surprising that the highly kinked steps we have examined show quite different results from straight steps, since several assumptions in the theoretical model of step fluctuations presented in section 3 fail for these steps. In particular, the kink density is not simply $\exp(-\varepsilon / k_B T)$ for these steps. It would be interesting to observe the transition from the observed $E_{eff}$ for highly kinked steps to the value for straight steps by simulating $(n,1)$ and $(1,n)$ steps with $n >> 1$. Unfortunately, $E_{eff}$ can only be accurately measured at temperatures where the deviations from power law scaling shown in Fig. 7 are absent. We have not been able to collect

sufficient high temperature data for steps such as (10,1) due to the extremely short time steps that must be used at these temperatures.

The enantiospecific adsorption properties of naturally chiral metal surfaces arise from the local ordering of atoms along step edges [1,3-5,7]. One preliminary way to assess the effect of step fluctuations on the local order in our simulations is to examine the step length distribution. We define $P_A(L)$ [$P_B(L)$] to be the probability that a randomly chosen A step [B step] segment has length $L$ between kinks. Figure 9 shows these distributions for a (3,1) step at $T = 500$ K. The equilibrium distribution is reached rapidly, even though the step's temporal correlation function continues to increase indefinitely [8]. The observed distributions after $t = 6$ minutes and $t = 1$ hour in Fig. 9 are almost indistinguishable. As might be expected, simulating a (1,3) step leads to very similar distributions with the roles of the A and B steps reversed. The equilibrium step length distributions, $P_A(L)$, for (1,1), (2,1) and (3,1) steps at 500 K are shown in Fig. 10. The results in Figs. 9 and 10 show that for these highly kinked steps the average step segment length increases during equilibration. That is, the kink density is reduced from its initial value once the step has equilibrated. This situation is the reverse of what happens for nominally straight steps, where the initial and equilibrium kink densities are nominally zero and $\exp(-\varepsilon/kT)$, respectively. The ratio of the average A and B step lengths is constant during roughening for each step, since the overall orientation of the step is fixed. For example, the ratio $\overline{P}_A : \overline{P}_B$ is initially 3:1 for a (3,1) step and is $4.15 \pm 0.13 : 1.39 \pm 0.04$ after $t = 1$ hour. This observation is important because it indicates that the net chirality of the step edge is retained, even though some local details of the step structure have been disrupted by the step roughening.

Submonolayer adsorption on chiral metal surfaces is dominated by molecules adsorbing in or near step kink sites [1,5-7]. It is therefore useful to characterize the kink sites that exist after step fluctuations occur. To do this, we denote by $m_B \rightarrow n_A$ a kink that is formed by a B (A) step of length $m$ ($n$) with the B step on the left when the step is viewed from above with the step bottom underneath the step edge. Using this notation, all the kinks in Fig. 1 are $1_B \rightarrow 3_A$ kinks. The mirror image of a $m_B \rightarrow n_A$ kink is a $n_A \rightarrow m_B$ kink. If a step has $m_B \rightarrow n_A$ and $n_A \rightarrow m_B$ kinks in equal proportion then the local chirality of these kinks will exactly cancel, leading to a set of kinks with no net enantiospecificity. Conversely, if either type of kink is present in excess of the other, adsorption on this set of kinks will be enantiospecific. For the (3,1) step discussed in Fig. 9, all kinks at $t = 0$ are $1_B \rightarrow 3_A$ kinks. Once the step's local structure has equilibrated ($t$ = 1 hour), the overall kink density is reduced to 69% of the original kink density and a diverse range of kinks exists: 43.3% are $1_B \rightarrow n_A$ with $n_A > 2$, 18.8% are $m_B \rightarrow n_A$ with $m_B > 1$ and $n_A > 2$, and 37.6% are $m_B \rightarrow n_A$ with $n_A \leq 2$. Crucially, less than 0.3% of the kinks are $n_A \rightarrow m_B$ for any $n_A$ or $m_B$. All the other kinked steps we have simulated behave similarly. This reinforces the observation above that the net chirality of these steps is maintained even though their local structure changes significantly as step fluctuations occur. Detailed models exist for the enantiospecificity of molecular adsorption at the types of kinks that can occur on Miller index surfaces [1,6-8]. We are currently working to extend these models to the range of kinks that we observe on kinked steps after thermal roughening [9]. Combining this work with the statistical descriptions of step structures just demonstrated will allow us to describe the enantiospecific

adsorption properties of naturally chiral surfaces both before and after thermally-driven step roughening.

**Section 5: Conclusion**

Naturally chiral metal surfaces exhibit enantiospecific adsorption properties due to the kinked steps that decorate these surfaces [1,2-7]. In this paper we have presented a model that will allow the impact of step fluctuations on these adsorption properties to be systematically studied. Our lattice gas model for step motions is derived directly from energy barriers computed using DFT, and yields good agreement with experimental measurements of straight Pt steps. We are currently working to combine the model presented here with models of molecular physisorption on chiral Pt surfaces [1,6-8].

We conclude by considering the physical limitations imposed by our model. Our model assumes that step fluctuations occur exclusively by periphery diffusion. All step fluctuations are expected to be dominated by mechanisms involving mass transport between steps at sufficiently long times [27,28]. Experimental observation of steps vicinal to Pt(111) has shown that periphery diffusion dominates for at least 10 seconds when T = 800 K [10] and for much longer times at lower temperatures (*cf.* Figs. 6 and 7). Our model is therefore appropriate for describing surfaces whose thermal history does not involve extended periods at very high temperatures. An additional restriction is that our model assumes adjacent step edges remain well separated at all times. This means that it is best used to describe chiral surfaces with wide terraces and correspondingly limited surface roughening. Although these restrictions mean we cannot yet provide a completely general description of Pt step roughening, they do not prevent us from providing useful information about the surfaces of interest in experimental studies of chiral surfaces. In

UHV studies of chiral metal surfaces [2,6], the surface temperature is below room temperature for the bulk of the experiment. The only portion of these experiments where the surface temperature is raised to the point where step fluctuations can occur at a significant rate is when the surface is briefly heated during cleaning. Thus, surfaces of interest can be generated by allowing an ordered structure to roughen for a limited period of time, a task for which our model is well suited, and subsequently quenching the surface to a temperature where the rate of adatom diffusion is essentially zero.

*Acknowledgments*: AA and DSS were supported by the National Science Foundation grant number CTS-9813937 and benefited from access to the PSC-CLAN at the Pittsburgh Supercomputer Center. PJF was supported by the U. S. Department of Energy under Contract DE-AC04-94AL85000. Sandia is a multi-program laboratory operated by Sandia Corporation, a Lockheed Martin Company, for the U. S. Department of Energy.

## References


[1] D.S. Sholl, Langmuir 14 (1998) 862.

[2] C.F. McFadden, P.S. Cremer and A.J. Gellman, Langmuir 12 (1996) 2483.

[3] A. Ahmadi, G. Attard, J. Feliu and A. Rodes, Langmuir 15 (1999) 2420.

[4] G. Attard, *et al.*, J. Phys. Chem. B 103 (1999) 1381.

[5] T.D. Power and D.S. Sholl, J. Vac. Sci. Technol A 17 (1999) 1700.

[6] J.D. Horvath, A.J. Gellman, D.S. Sholl and T.D. Power, in: Physical Chemistry of Chirality, ed. J. Hicks (ACS Symposium Series, 2000) in press.

[7] T.D. Power and D.S. Sholl, submitted to this issue of Topics in Catalysis.

[8] H.-C. Jeong and E.D. Williams, Surf. Sci. Rep. 34 (1999) 171.

[9] D.S. Sholl, A. Asthagiri and T.D. Power, in preparation.

[10] M. Giesen, G.S. Icking-Konert, D. Stapel and H. Ibach, Surf. Sci. 366 (1996) 229.

[11] E. Hahn, H. Schief, V. Marsico, A. Fricke and K. Kern, Phys. Rev. Lett. 72 (1994) 3378.

[12] P.J. Feibelman, Phys. Rev. B 60 (1999) 4972.

[13] P.J. Feibelman, unpublished results.

[14] N.C. Bartelt, T.L. Einstein and E.D. Williams, Surf. Sci. 312 (1994) 411.

[15] Th. Michely and G. Comsa, Surf. Sci. 256 (1991) 217.

[16] P.J. Feibelman, Surf. Sci. Lett., in press.

[17] N.C. Bartelt, J.L. Goldberg, T.L. Einstein and E.D. Williams, Surf. Sci. 273 (1992) 252.

[18] A. Pimpinelli, J. Villian, D.E. Wolf, J.J. Metois, J.C. Heyraud, I. Elkinani and G. Uimin, Surf. Sci. 295 (1993) 143.

[19] M. Giesen-Seibert, F. Schmitz, R. Jentjens and H. Ibach, Surf. Sci. 329 (1995) 47.

[20] A. Natori and R.W. Godby, Phys. Rev. B 47 (1993) 15816.

[21] D.S. Sholl. and R.T. Skodje, Phys. Rev. Lett. 75 (1995) 3158.

[22] P.J. Feibelman, Phys. Rev. Lett. 81 (1998) 168.

[23] D.W. Bassett and P.R. Webber, Surf. Sci. 70 (1978) 520.

[24] A.B. Bortz, M.H. Kalos and J.L. Lebowitz, J. Comp. Phys. 17 (1975) 10.

[25] M. Giesen, Surf. Sci. 442 (1999) 543.

[26] S.V. Khare and T.L. Einstein, Phys. Rev. B. 57 (1998) 4782.

**Figure Captions**

Figure 1: A ball model of Pt(854) with step edges highlighted by solid lines.

Figure 2: An island on a Pt(111) surface illustrating the atom types used in our extended bond counting model.

Figure 3: A schematic illustration of the coordinate system used to define G(t) for a kinked step. The solid line indicates the initially ordered step edge and the dashed line indicates the step position at a later time.

Figure 4: The potential energy surface assumed by Giesen *et al.* [10] for diffusion of an adatom along a step edge past a kink site (K).

Figure 5: The potential energy surface for a Pt atom diffusing along an A step as determined using DFT [12]. Barriers indicated without (with) parentheses were computed using LDA (GGA) with energies in eV.

Figure 6: The step temporal correlation function, *G(t),* for a (3,1) Pt step. Fromleft to right, the data are for $T = 550$, 500, and 450 K. The straight lines are least squares fits to $G(t) \propto t^{\alpha}$.

Figure 7: The same as Fig. 6 but for a (10,1) Pt step with $T = 700$, 650, and 600 K from top to bottom.

Figure 8: An Arrhenius plot of $G(t)$ with $t = 1$ hr for $(n,1)$ Pt steps. The effective energy barriers determined from this data, $E_{eff}$, are indicated.

Figure 9: Step length distributions, $P_A(L)$ (circles) and $P_B(L)$ (triangles), for a (3,1) Pt step at $T = 500$ K. The filled (open) symbols show data taken with $t = 6$ minutes (1 hour).

Figure 10: Step length distributions, $P_A(L)$, for $(n,1)$ Pt steps at $T = 500$ K and $t = 1$ hour.

**Table 1:** Energy barriers from LDA (GGA) DFT calculations [Feibelman99] and as predicted using Eqs. (AA) and (BB). A, B, C, and K represent energy minima at A-step, B-step, corner, and kink sites on high Miller index surfaces, respectively.

| Transition | DFT $E_b$ (eV) | Predicted $E_b$ (eV) | Difference (eV) |
|---|---|---|---|
| A → A | .84 (.71) | .857 (.714) | .017 (.004) |
| A → K | .85 (.71) | .845 (.713) | -.005 (.003) |
| K → A | 1.27 (1.01) | 1.32 (1.07) | .05 (.06) |
| A → C (-K) | .96 (.82) | .922 (.783) | -.038 (-.037) |
| A → C (-B) | .99 (.84) | .922 (.783) | -.068 (-.057) |
| (K -) C → A | .51 (.46) | .447 (.405) | -.063 (-.056) |
| (B -) C → A | .49 (.44) | .447 (.405) | -.043 (-.036) |
| (A -) C → K | .45 (.42) | .427 (.382) | -.023 (-.038) |
| B → B | .90 (.77) | .903 (.775) | .003 (.005) |
| B → K | .90 (.77) | .889 (.760) | -.011 (-.011) |
| K → B | 1.41 (1.18) | 1.34 (1.11) | -.066 (-.07) |
| (B -) C → K | .39 (.35) | .429 (.396) | .038 (.046) |
| (K -) C → B | .40 (.37) | .449 (.419) | .049 (.049) |
| (A -) C → B | .40 (.38) | .449 (.419) | .049 (.039) |
| B → C (-K) | .89 (.74) | .944 (.800) | .054 (.060) |
| B → C (-A) | .90 (.77) | .944 (.800) | .044 (.030) |
| K → C (-A) | 1.32 (1.08) | 1.35 (1.10) | .03 (.02) |
| K → C (-B) | 1.39 (1.13) | 1.37 (1.12) | -.02 (-.01) |

**Table 2:** Parameters used in Eqs. (AA) and (BB) parameterized using barriers computed using LDA and GGA.

| Method | $\gamma$ | $E_A^{TS}$ | $E_B^{TS}$ | $E_{120}^{TS}$ | $E_{240}^{TS}$ | $E_A^{TS}$ | $E_B^{TS}$ | $E_{120}^{TS}$ | $E_{240}^{TS}$ |
|---|---|---|---|---|---|---|---|---|---|
| LDA | .5 | -.047 | -.044 | -.041 | -.029 | -.475 | -.495 | -.45 | -.50 |
| GGA | .5 | -.022 | .006 | -.045 | .020 | -.379 | -.381 | -.34 | -.395 |

**Table 3**: Values of the scaling component, $\alpha$, for different step structures (n,m).

| n | m | $\alpha$ (T=450K) | $\alpha$ (T=500K) | $\alpha$ (T=550K) |
|---|---|---|---|---|
| 3 | 1 | .213 +/- .009 | .230 +/- .016 | .234 +/- .007 |
| 2 | 1 | .225 +/- .005 | .218 +/- .003 | .231 +/- .012 |
| 1 | 1 | .236 +/- .020 | .224 +/- .012 | .235 +/- .013 |
| 1 | 2 | .236 +/- .019 | .226 +/- .005 | .224 +/- .003 |
| 1 | 3 | .221 +/- .023 | .229 +/- .018 | .219 +/- .012 |

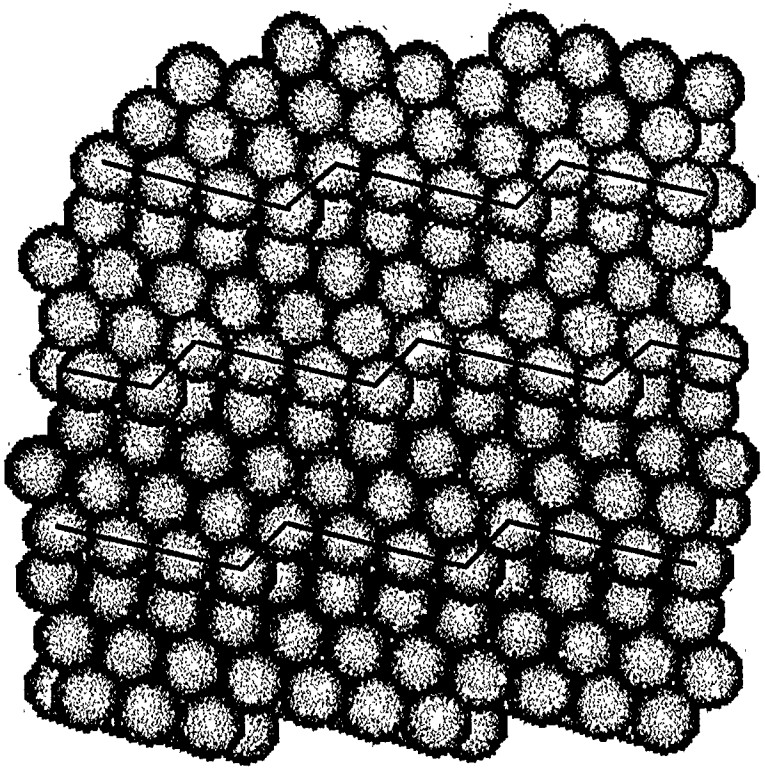

Asthagiri, Feibelman, and Sholl

Fig. 1

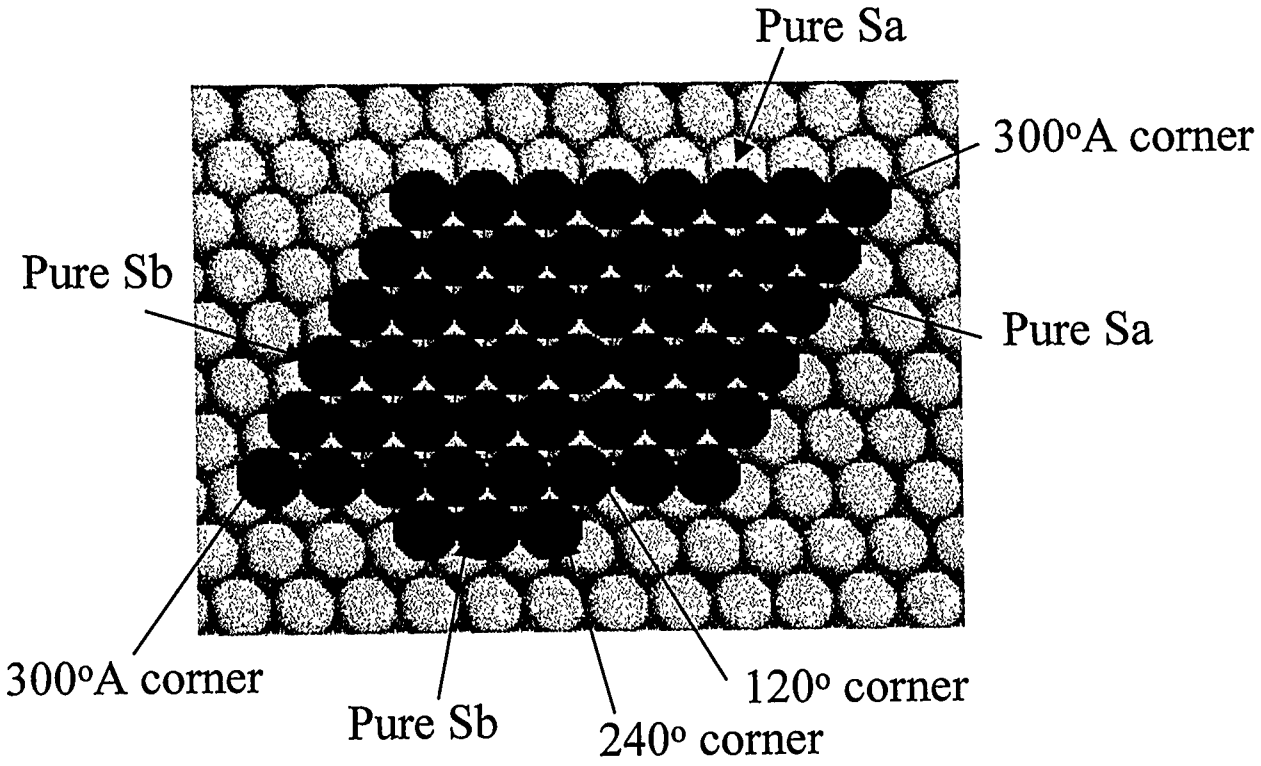


Asthagiri, Feibelman, and Sholl

Fig. 2

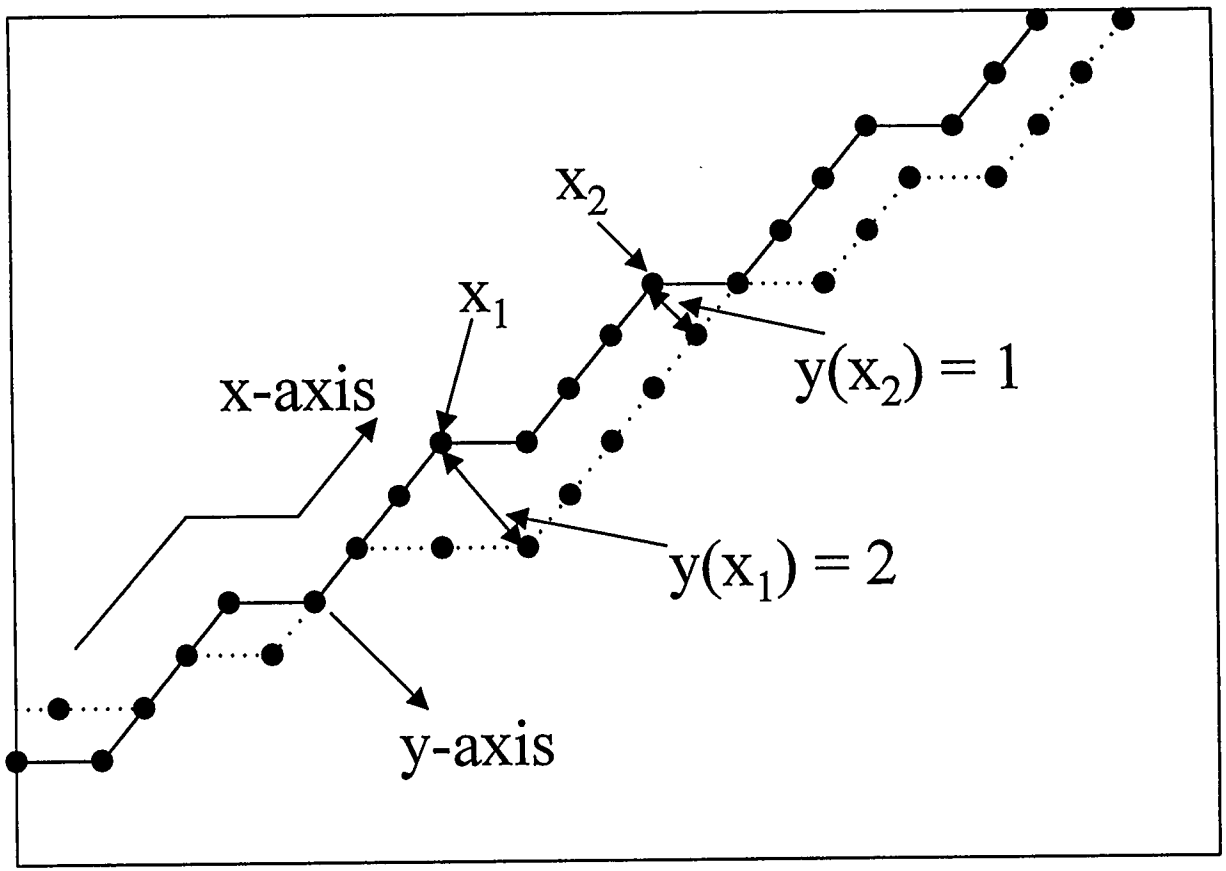


Asthagiri, Feibelman, and Sholl

Fig. 3

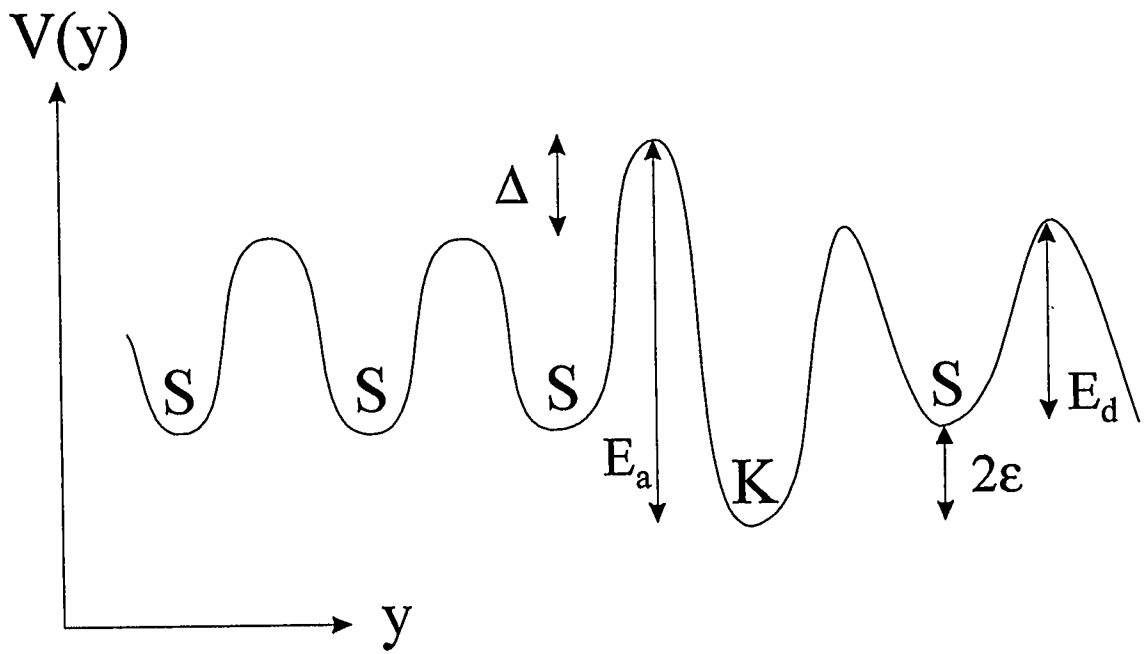


Asthagiri, Feibelman, and Sholl

Fig. 4

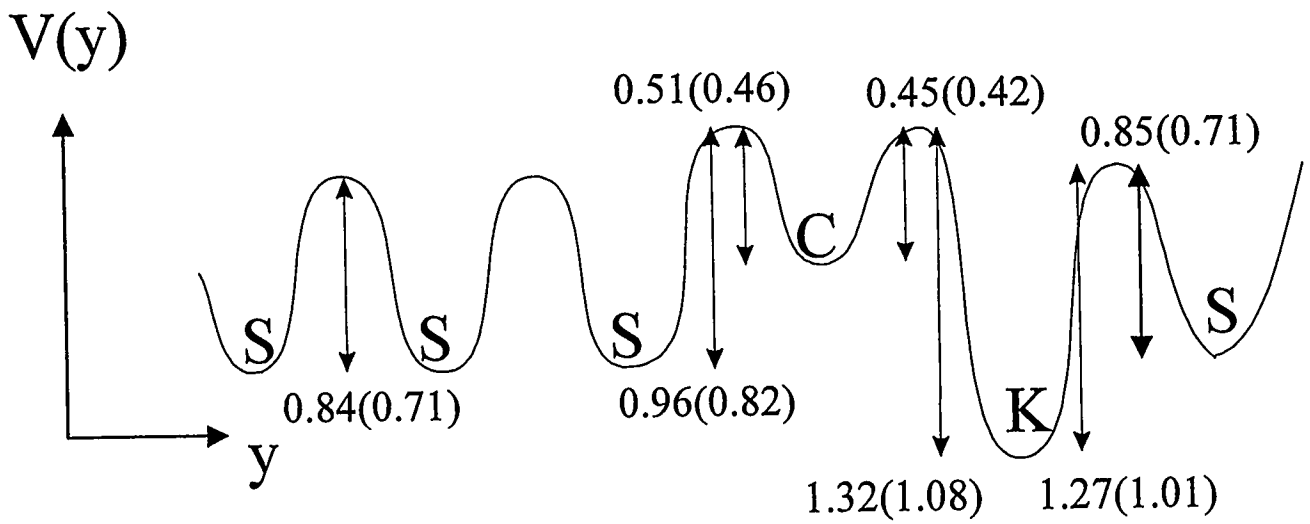


Asthagiri, Feibelman, and Sholl

Fig. 5

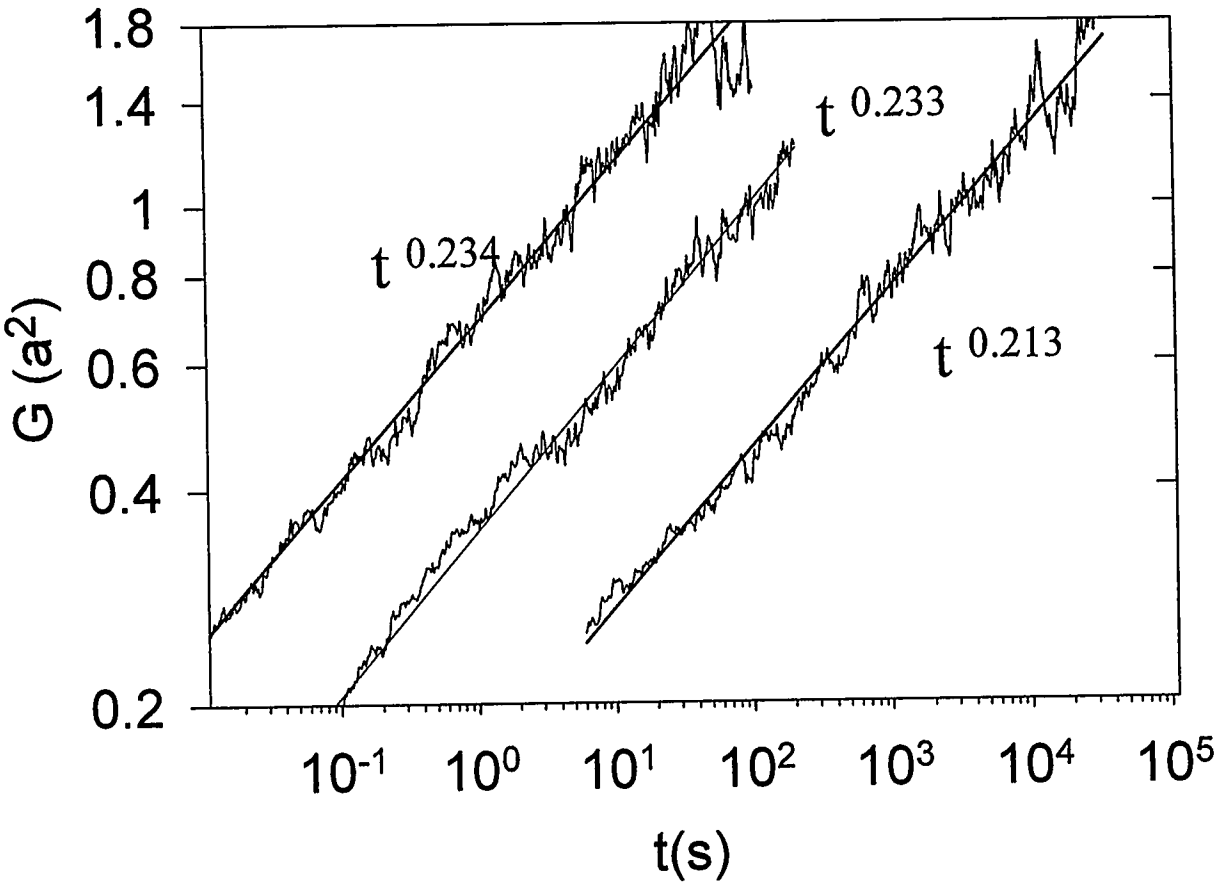


Asthagiri, Feibelman, and Sholl

Fig. 6

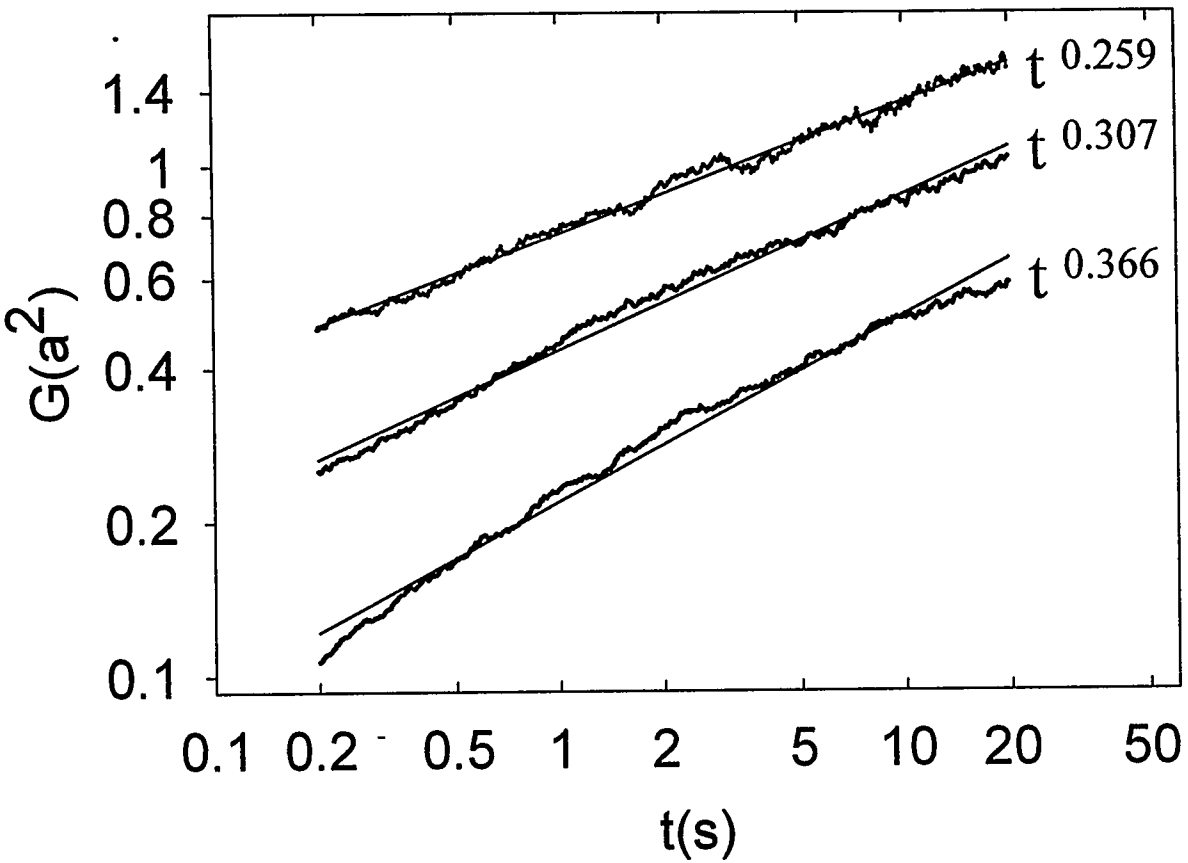


Asthagiri, Feibelman, and Sholl

Fig. 7

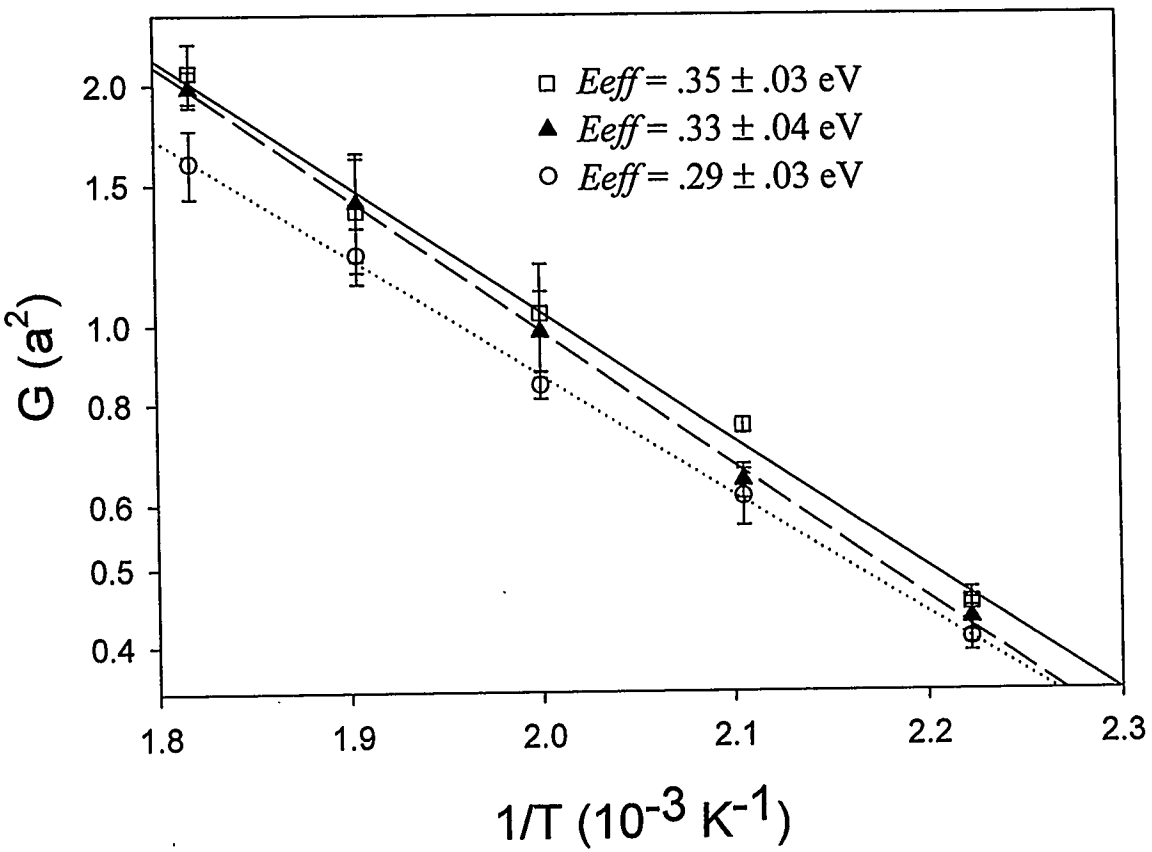


Asthagiri, Feibelman, and Sholl

Fig. 8

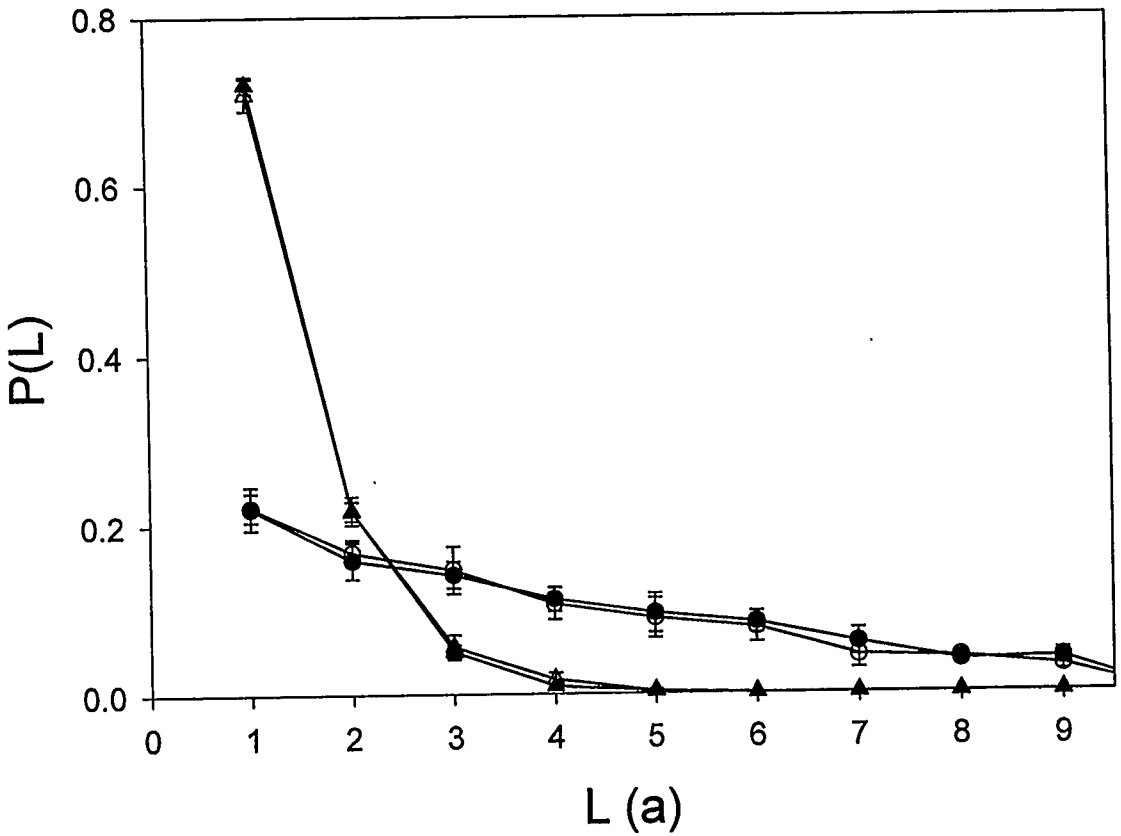


Asthagiri, Feibelman, and Sholl

Fig. 9

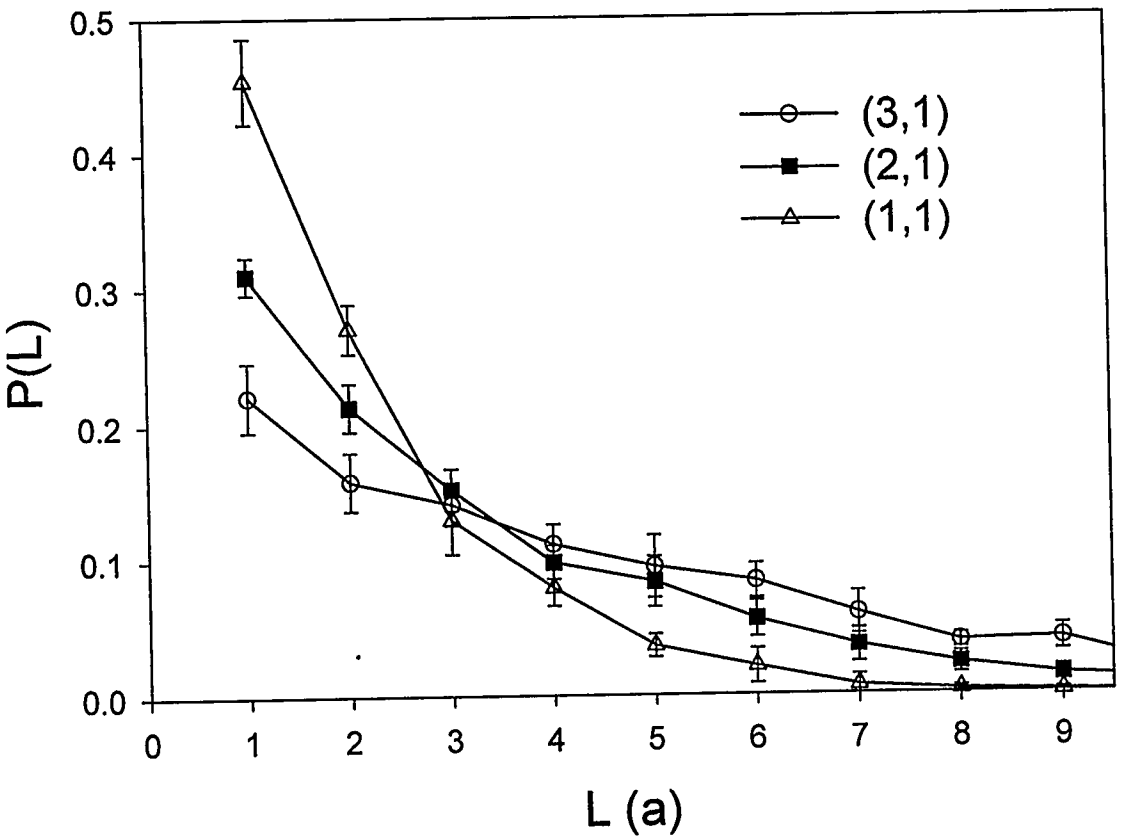


Asthagiri, Feibelman, and Sholl

Fig. 10